

Experimental set up for *in situ* Transmission Electron Microscopy observations of chemical processes

Renu Sharma

Center for Nanoscale Science and Technology, National Institute of Standards and Technology,
Gaithersburg, MD 20899-6203

Abstract

Recently, the applications of transmission electron microscopy (TEM) related techniques have extended from *ex situ* nanoscale characterization of structure and chemistry of products to dynamic measurements of nanostructures during reaction processes. Commercially available modified TEM specimen holders and TEM columns are being routinely employed to follow the structural and chemical changes at elevated temperatures and even under controlled atmosphere. Experiments performed under these rigorous conditions require careful considerations to avoid undesirable effects from the gas impurities or contaminations from TEM grids and/or holders. The reactivity of sample, grid, holder, TEM components, and gaseous environments must be evaluated for each reaction process. This tutorial is aimed to outline some of the important factors that should be considered for experimental set up used for *in situ* observations to ensure the results are comparable to the ones obtained during *ex situ* experiments under identical conditions.

Highlights:

- Advantages and limitations of *in situ* heating experiments using TEM are outlined.
- Sources of contamination and adverse reactions are identified.

- Important considerations for planning *in situ* experiments that can replicate *ex situ* experimental results are outlined.
- Temperature and pressure response to reactivity of sample and TEM components is explained.
- Detailed explanation for planning experimental conditions and choosing suitable TEM based data acquisition technique is provided.

Keywords: *In situ* TEM, environmental (scanning) transmission electron microscope (E(S)TEM), catalysis, nanowires, nanotubes.

1. Introduction:

Historically transmission electron microscopy (TEM) has been used as one of the most powerful *ex situ* techniques for atomic scale characterization of structure and chemistry of solids, especially of nano-structured materials. The concurrent acquisition of atomic resolution images and nanoscale chemical analysis, from samples before and/or after synthesis provides information about the relationship between reactants and products that can be employed to deduce possible reaction mechanisms. In the seventies, electron beam irradiation was often employed to initiate sintering of nanoparticles or phase transformations (Bovin and Malm 1991). Currently, single-tilt and double-tilt heating stages are commonly used to perform controlled heating experiments. However, information about the structural and chemical changes occurring under ambient conditions, especially under gaseous environment, is generally missing as TEM operates under high vacuum conditions. Similarly, the evaluation of the effect of external stimuli such as mechanical (stress), electrical and magnetic force applied during operation, on the

nanomaterials or their ensemble cannot be determined using *ex situ* imaging and spectroscopy techniques. Therefore, a number of modifications to TEM sample holders and to TEM columns have been implemented over the years that are now routinely used for *in situ* measurements of the structure, morphology, chemistry and properties of nanomaterials under reactive conditions.

During the last couple of decades, researchers have recognized the value of *in situ* characterization of nanostructured materials using TEM based techniques. The need for nanoscale measurements stems from the rigorous control of synthesis conditions that are essential for nanofabrication. Continued progress in nanotechnology requires a bottom-up approach, where synthesis of nanoscale components is a part of nanofabrication and nanomanufacturing. Moreover, the properties of nanomaterials are often controlled by their nanoscale structure and morphology, and any modification to them, occurring during the operation, will adversely affect their performance. Hence, the *in situ* nanoscale characterization is essential not only to optimize synthesis process of nanomaterials but also to determine the conditions for their optimum performance. Some of the advantages of *in situ* TEM observations are:

1. The same area or the same nanoparticle is observed before, during and after being subjected to external stimuli. Therefore, all reaction steps, including intermediate steps (if any), may be identified if the life of the reaction intermediates is longer than the data acquisition rate.
2. Careful design of the experiments enables observation of structural, morphological and chemical changes concurrently.

3. Measurement of both the thermodynamic and the kinetic data for the reaction processes leading to nanomaterials synthesis and/or functioning can be obtained.
4. A direct relationship between structure and properties is determined.
5. *In situ* observations result in considerable time saving as the synthesis and characterization is performed concurrently.

Clearly the insight provided by *in situ* observations can be exploited to facilitate robust scaling of nanoscale synthesis processes to the manufacturing levels. In recent years, the number of publications describing the instrumental development and their applications has exponentially increased and several review articles (Sharma 1998; Sharma 2005; Sharma 2005; Yao 2005; Stach 2008), special journal issues (1998; 1998; 2005; 2008; 2009), and books (Gai 2003; Yao 2005; Barnhart 2008), have been published on this topic and will not be discussed here.

Although most of the published literature provides detailed description of the set-up employed for successful *in situ* experiments, information about planning strategies for these experiments is lacking. It is important to note that the modified TEM column and/or sample holders, used for *in situ* characterization, should be treated with the same considerations as for a synthesis furnace or chemical vapor deposition reactor since the TEM is no longer used only as characterization tool. This paper aims to provide a tutorial concerning the most common considerations required for successful *in situ* observations during heating experiments in vacuum or gaseous environments in a TEM.

2. Reactivity of various components

As TEM samples are loaded in a heating holder and may also require additional support, it is imperative to have an in depth understanding of the chemical nature of individual components and their reactivity as explained in following sections.

2.1. Reaction of grid/support materials with sample and/or each other

Generally carbon films or lacey supports on metal grids, used to load the samples for TEM observations, are most suitable to load powder samples as they provide support but have negligible influence on structural image formation. However, the catalytic reaction can be influenced by the nature of the support film due to metal-support interaction (MSI). Moreover, the reactivity of support films is also influenced by the nature of the ambient. For example, Ni nanoparticles have been reported to graphitize carbon thin films at 600 °C (Anton, 2008). Similar catalytic graphitization of amorphous carbon by 500 nm Ni particles has also been reported to occur under a focused electron beam (Aikawa al., 2010). Amorphous carbon support films are also prone to break during heating due to thermal stress and will burn off (oxidize) when heated in an oxygen environment. As a result, the area under investigation may be lost and the experiment will fail to provide conclusive results. Silica (SiO_x) thin films may be used as an alternative support, especially to study catalytic processes. The powder samples containing nanoparticles may also be directly loaded on the metal grids, thereby avoid a support film. In this case the sample will attach to the grid bars due to electrostatic forces and the particles sticking out in the vacuum, away from the grid bars will be suitable for *in situ* observations. However, in this case the chemical nature of the grid becomes important and should be selected after careful considerations as explained below.

Cu is the most commonly used grid material but other metals, such as Ni, Al, Mo, Pt, Au and stainless steel are also available. For *in situ* heating, the physical and the chemical properties of the grid material must also be considered. First and foremost, the choice of grid material is dependent on the desired reaction temperature. Obviously Cu grids should not be used for heating samples above its melting point (1084 °C). Additionally, it has been shown that metal atoms start to diffuse at temperatures as low as half the melting temperature in Kelvin (Taman temperature), which is ≈ 400 °C for Cu (Zhang and Su, 2009). The diffusion of metal atoms onto the samples near or above the Taman temperature can be considered as an addition of a contaminant to the reactants. As the sample is in direct contact with the grid material, the addition of metal particles described above can affect the reaction mechanism.

Zhang et al. (Zhang and Su, 2009) have tested the stability of Cu, Ni, Mo, and Au TEM grids, coated with ultra-thin films of α -C or SiO_x, in the temperature range of 500 °C and 850°C. They have found that although different metals and supports behaved differently, most of the grid materials adversely changed the structure of the support material above 600 °C. For example, Cu particles were observed to nucleate (Fig. 1) on amorphous (α)-C film at 600 °C either due to evaporation and re-deposition or due to surface mobility above the Taman temperature (≈ 400 °C). They have also shown that the nature of the support film also plays a role in the formation of metal particles of the grid material.

We have found that the yield of carbon nanotube (CNT) formation increased noticeably at 490 °C when Ni/SiO₂ catalyst was loaded directly onto Au instead of Ni grids, as shown in Fig. 2.

We believe that since our reaction temperature is above the T_{sublimation} temperature for Au (≈ 396 °C), some Au atoms diffused to the catalyst particles and changed their reactivity. Our controlled experiments and theoretical simulations have confirmed that a small amount of Au doping in Ni catalysts improves the CNT yield (Sharma et al., 2011).

Low amounts (0.2 $\mu\text{mol/mol}$) of nickel carbonyl, a volatile product that is a health hazard, have been reported to form when a Ni single crystal was exposed to CO at low temperatures (Lascelles and Renny, 1983). However, this reaction may not have any adverse effects on the reaction process under observation as the rate of formation is very low (2×10^{-9} mole per cm^2 per min at 130 °C) and its effect is further diminished by the fact that it decomposes above 350 °C.

2.2. Gas purity

It is self-evident that we need to use high purity gases to make sure that impurities do not affect the reactions path. However, for some gasses this is detrimental for the success of the experiment. For example, presence of small amount of water vapor in hydrogen will alter the oxygen chemical potential in the gas volume; thereby lower its reducing property. Generally, a liquid nitrogen trap on the line between gas tank and inlet to mixing chamber or ETEM column is used to freeze out the moisture. However this method to remove water is applied only if the boiling point of the experimental gas is below the LN₂ temperature. Other filters must be used for gasses such as ammonia that will liquefy at this temperature.

Active Coke filter is also often used with carbon monoxide (CO) if purchased in steel cylinder to remove contaminants, especially iron carbonyl species. Alternatively, CO in aluminum tank should be used to study catalytic processes such as Fischer Tropsch reaction.

2.3.Reaction of the environment with TEM heating holder

Next, we need to consider the materials used to build the heating holders and their components. The composition of the heating holder controls the temperature and environments suitable for its use. The reactivity of gaseous environment must be considered for planning *in situ* observation of gas-solid interactions in an environmental scanning transmission electron microscope (ESTEM) as some of the gasses may adversely affect the components of the TEM holders, such as the body of the heating furnace, washers, wiring material, etc. Detailed information about the nature of the materials may be readily available and should be used to select the experimental condition. Some of this information may be proprietary and therefore not readily available. In this case, the manufacturer should be consulted to make sure that the liquids or gases to be used or produced during the reaction will not harm the instrumental components. For example, Ta heating holders will oxidize when exposed to oxygen or air, and Pt heating or thermocouple wires will form silicides when heated above 300 °C in the presence of silane (Takahashi, Ishii et al., 1985). Also, consult the relevant phase diagrams to make sure that the experiments can be safely performed using the available instrumentation.

Kamino and Saka (1993) have developed a holder where a thin tungsten wire can be heated up to 1500 °C by resistive heating. A modified version of this holder, called a gas-injection holder

allows small amounts of gas to be introduced in the sample area. (Kamino [et al.](#), 2005) Both of these holders are stable and can be used to obtain atomic resolution images at high temperature. However, users must consider the reactivity of tungsten with the sample under observation as well as with the environment prior to using it for *in situ* experiments. Chen and Mori (Chen and Mori, 2009) have reported the formation and growth of $W_{19}O_{49}$ nanowires over time when a tungsten wire was heated to 600 °C in high vacuum (10^{-4} Pa) as shown in Fig. 3a-c. High-resolution images (Fig. 3d) show that these wires are perfectly crystalline with growth direction along $\langle 010 \rangle$. It is well known that oxidation of tungsten requires very low oxygen partial pressure. Also, tungsten oxide nanowires have been reported to grow via vapor solid-solid growth mechanism (Kojima [et al.](#), 2008). The growth of oxide nanowires reported by Chen and Mori (Chen and Mori, 2009) indicates that high vacuum conditions in the TEM have enough oxygen partial pressure to oxidize tungsten upon heating. It is also possible that the water vapor present in the column may be responsible for the vapor transport and growth of $W_{19}O_{49}$ nanowires as reported by Sahle (Sahle and Berglund, 1981). The important conclusion to be drawn from this report is that the low oxygen partial pressure, existing under the high vacuum conditions of the TEM column, can be sufficient to oxidize certain metal grids and should be taken in to account while choosing the grid material. It may be concluded that an ultra-high vacuum TEM column will be more suitable for tungsten wire holders.

2.4. Temperature and pressure considerations

The maximum achievable temperature primarily depends upon the modified heating holder and varies between 1000 °C and 1500 °C, depending upon the source and design (Kamino [and Saka](#),

1993; Allard [et al.](#), 2009). The steady-state temperature at the sample using these holders is stable enough to capture atomic resolution images in TEM and STEM modes. Heating holders are also commercially available with approximately the same temperature range. However the practical temperature range available is controlled by the (a) grid material and (b) chemical nature of the gas environment to be used. Neither the grid material nor the gas should react with the body of the heating holders under the experimental conditions.

The components of the TEM column and the heat capacity of the gas will also limit the highest achievable temperature as some of the internal components of the commercially available differentially pumped ETEMs or ESTEMs cannot withstand high temperatures. The heat transfer from the sample and the holder to the other parts in the TEM column may occur due to the gas convection. The heat transport by a gas can be calculated using the following equation:

$$\Delta H = 2\mu_a(T_s - T_g)$$

where μ_a is the heat capacity of the gas, T_s and T_g are the sample and gas temperature, respectively. When a gas at room temperature is introduced in the TEM column, it will transport heat from the sample to the other parts of the TEM column. As a result the sample will cool down and other parts of the column may be heated. This conductive heating depends upon the temperature difference ($T_s - T_g$), the heat-capacity of the gas (μ_a), gas pressure, distance from the sample and the time. The rate of heat transfer in a static flow system can be calculated using the general equation for heat transfer:

where Q is heat transfer, t is time, and h is the convective heat transfer coefficient, A is the surface area for heat transfer and ΔT is temperature difference. The convective heat transfer coefficient is dependent upon the physical properties of the gas and the flow regime, i.e., laminar or turbulent. As the O-ring seals, currently being used to hold differential pumping apertures in place, in the upper and lower pole-piece bore, cannot be heated beyond 200 °C (<http://www.marcorubber.com/viton.htm>), the upper temperature should be calculated for individual experiment. Currently the recommended temperature in a modern commercial E(S)TEM with gas flow is 1000 °C, even if the heating holder is capable of achieving higher temperatures.

Gas heat capacity and pressure will also affect the electrical current required to achieve the reaction temperature by resistive heating. Compared to the vacuum, higher current is necessary to heat up the sample in a gaseous environment because gases are usually admitted at room temperature and are sources of considerable heat loss due to conduction and/or convection. Again, the amount of additional heating current required depends on thermal conductivity and pressure of the gas in the cell. Table 1 gives the thermal conductivities of gases that are often used in E(S)TEM experiments. This table shows that the thermal conductivity for H₂ is extremely high so that high temperature work will require significantly higher heating currents. If possible, it is advisable to achieve the required reaction pressures before heating the samples, as the gas flow will drastically cool down the sample due to conductance (Table. 1). The thermal conductivity of H₂ can be reduced by mixing it with inert gases such as Ar or N₂ (Table. 1).

The highest available pressure in the sample region is usually restricted by the instrumentation design. Generally a very low gas pressure, in the order of a few Pa, is permitted in a gas injection system (Ross, ~~Tromp~~ et al., 1999; Kamino [et al.](#), 2005). On the other hand the highest achievable gas pressure in a differentially pumped TEM column is dependent on the pumping speed of the system, which in turn depends on the nature of the gas as well as the design of the pumping system (Robertson [and Teter](#), 1998; Gai, 1999 ; Sharma, 2005). The current limit for nitrogen in a commercially available differential pumped TEM is $\approx 2 \times 10^3$ Pa (20 mbar). Again, this value will change depending on the conductivity of the gas. The pressure for windowed gas reaction TEM holders is higher and depends upon the design of the holder. Creemer et al. (Creemer, ~~Helveg~~ et al., 2008) have obtained atomic resolution images at 1.2 bar of H₂ pressure at 500 °C using such a holder.

For a particular experimental set up, the temperature and pressure are controlled by the thermodynamic conditions required for a chemical process of interest to occur. For example, NiO can be reduced in high vacuum conditions (10^{-2} Pa) at ≈ 500 °C (Gajdardziska-Josifovska [et al.](#), 2002), but CeO₂ reduction will occur at temperature above 1600 °C (Bevan, 1955), However, the reduction temperature of both these oxides can be reduced to 270 °C (Richardson et al, 1994), and 800 °C (Sharma [et al.](#), 2004) respectively, when heated in 200 Pa of hydrogen instead of vacuum.

2.5. Switching or mixing gasses

Switching gases or mixing two gases is often required for initiating or evaluating certain catalytic processes. For example, oxygen and hydrogen flows will be alternated to follow redox behavior of a number of oxides such as ceria (CeO_2) or iron oxide (Fe_2O_3). An abrupt change of gasses with different heat capacities (μ_a and μ_b) will unbalance the thermal equilibrium of the system. As a result the temperature may shift to a different reaction regime and if μ_a is greater than μ_b , then the resulting sample temperature increase may damage the holder or TEM components. Sudden temperature changes will also cause significant sample drift for an extended period of time making it hard to capture images, diffraction patterns or spectroscopy data. One of the solutions to the problem is to introduce an inert gas, such as N_2 or Ar as a buffer between the switching. For example, the amount of N_2 in oxygen can be slowly increased while decreasing the oxygen flow such that the thermal conditions of the system are maintained. After, a suitable period of pure N_2 flow, hydrogen may be slowly added to the replace the N_2 .

The above mentioned experiment will require mixing of two gases, i.e. O_2 and N_2 or H_2 or N_2 . Crozier and Chenna (2011) have followed the composition of gas mixtures in the ESTEM column using electron energy-loss spectroscopy (EELS) and found that the gas first added to the mixing tank effectively reduced the diffusion of the second gas through the inlet line, delaying homogeneous mixing along the line. It is interesting that, even when a highly mobile gas like H_2 is involved, it takes an hour to reach equilibrium composition in the sample region. Fig. 4 shows the time-resolved low-loss EELS collected after introduction of O_2+H_2 mixture from a mixing tank. The tank was first filled with 6.7×10^4 Pa of O_2 and then 3.34×10^4 Pa of H_2 was added to it. The mixture was then immediately admitted into the TEM column and time resolved spectra were recorded. The H_2 plasma peak at 12.5 eV (Fig. 4a) continuously increased in intensity (Fig.

4b) until the equilibrium pressure in the mixture was attained after about 60 min (Fig. 4c). The time required to reach this equilibrium condition will depend on the nature, pressure, flow rate and order in which the gases are introduced in the mixing tank as the system is essentially in what is referred to as a ‘‘plug flow’’ regime in reactor engineering (Crozier and Chenna, 2011).

3. Example of experiment planning:

From the above discussion it may appear that it is almost impossible to perform successful *in situ* heating experiments, but we know that the results from such experiments are reported routinely. Planning heating experiments is comparatively easy in vacuum than in gaseous environment as introduction of gas increases the number of parameters to be considered, not only due to their chemical nature but also due to the physical parameters such as heat capacity and diffusion rate. The examples described here for nanowire growth may be treated as general guidelines for planning experiments in an E(S)TEM.

Both E(S)TEM and high vacuum TEM (HVTEM), incorporated with gas handling systems, have been successfully utilized to elucidate the nucleation, growth mechanism and reaction kinetics of Si, Ge and GaN nanowires (Kodambaka, Tersoff et al., 2006; Kodambaka et al., 2007; Hofmann et al., 2008; Gamalski, Tersoff et al., 2010). In order to plan an *in situ* experiment, we must first consider both the desired and undesired reactions. One of the most effective ways to explore them is to examine the phase diagram. For example, Au-Si has a eutectic point at 360 °C for 0.2 mol/mol of Si in Au, therefore for the silicon nanowire to form via vapor-liquid-solid growth mechanism the growth temperature must be above this eutectic temperature (Fig. 5a). On the

other hand from the Pt-Si phase diagram we note that platinum silicide formation can start at temperatures as low as 400 °C (Okamoto, 1995). This is an undesired reaction and restricts the use of a heating holder with Pt heating or thermocouple wires. We also find that Si nanowires grow Pd nanoparticles by the vapor-solid-solid mechanism (Hofmann [et al.](#), 2008); therefore the growth temperature can be selected to be below the first eutectic point (835 °C) in the Pd-Si phase diagram (Fig. 5b).

Planning an *in situ* growth experiment for GaN nanowires in an E(S)TEM is more complicated as the nucleation and growth is a two-step process; first a Au-Ga melt is formed above the eutectic temperature, next liquid Ga reacts with ammonia (NH₃) to form solid GaN nanowires. Moreover, direct nitridation of Ga will happen only in the liquid Au-Ga droplet. Therefore, we need to define conditions that are favorable for both steps. For the first step, the phase diagram (Fig. 6a) can be used to determine the relationship between the desired Au-Ga ratio in a particle and the temperature of growth. We find that the Au-Ga liquidus line spans from 0.22 mol/mol Au in Ga to almost pure Ga above 500 °C. Next, we need to consider the conditions required for the nitridation reaction. It is well known that nitrogen produced during the dissociation of NH₃ has higher activity for nitridation reactions than for pure N₂ but the reaction temperature needs to be higher than the onset temperature of NH₃ dissociation (650 °C) (White and Melville, 1905). Therefore, we prepared samples with ≈ 0.5 mol/mol of Ga in Au for *in situ* nitridation and nanowire growth and heated to 700 °C (Diaz [et al.](#), 2012). However, we found that local variations in composition resulted in a distribution of active (liquid alloy) and inactive (solid) particles. Sometimes a liquid particle (Fig. 6b) was observed to dissolve more Au from the matrix and become solid (Fig. 6c) and thereby inactive.

4. Selecting appropriate characterization technique(s)

It is important to note that all of the TEM-related techniques such as imaging (bright field, dark-field, low and high resolution), diffraction (selected area, convergent beam, and nano-diffraction), scanning transmission electron microscopy (annular dark-field and high angle-annular dark-field), electron energy-loss and energy-dispersive spectroscopy (EELS and EDS), tomography, holography, etc. can be used for *in situ* observations. Some of these techniques can be combined within the same experiment, depending upon the temporal resolution of the desired technique relative to the reaction rate of the chemical process under observation. Ideally, we should combine more than one technique to unequivocally identify each step of the reaction process. For example, structural transformations can be followed either from time and temperature resolved electron diffraction (Schoen, Peng et al., 2009) or high-resolution images. (Sharma et al., 2009) On the other hand we need to collect spectroscopy data to determine the chemical changes (Sharma et al., 2004; Crozier and Chenna 2011). Examples given here can be used as guides for selecting a technique or a set of techniques that should be used to obtain as much information as possible for a given *in situ* experiment. However, we should keep in mind that the power of *in situ* TEM lies in providing atomic-scale information on the reaction mechanism, the relationship between local composition and reactivity, and the relationship between local structure and properties etc. and not the bulk behavior.

5. Recording media

Our ability to obtain useful information from *in situ* TEM imaging or spectroscopy data is strongly dependent upon available temporal resolution of the recording media. Both digital and analog cameras, currently available to record high-resolution images, are limited to frame rate of $\approx 30 \text{ s}^{-1}$ (fps). Recently, new cameras based on CMOS technology with possibility to record images at frame rate of 200 s^{-1} (fps) have been introduced (Litwiller, 2005). But their feasibility for recording atomic resolution images is yet to be tested. Improving the time resolution for HREM imaging is not a trivial challenge as it depends upon both the detector efficiency and electron dose (Alani and Pan, 2001). Typical electron beam currents for HREM imaging are between 1 nA and 10 nA; assuming recording takes place at a video rate of 30 frames s^{-1} or $\approx 0.033 \text{ s}$ per frame, the number of electrons per frame is between 6×10^9 and 6×10^{10} . Assuming images have the standard National Television System Committee (NTSC) resolution of 440×480 pixels, there is an average of 750 electrons per pixel and one wants to detect a minimum of 8 contrast levels, then 64 electrons per pixel would be necessary on a perfect detector. However, typical detector quantum efficiencies (DQEs) for camera are between 0.07 and 0.7 across the spatial frequency and kV range of interest, thus requiring between 100 and 1000 electrons per pixel. This means that, at the resolution and sensitivity of current cameras, we are already at (or close to) the practical limit of frame rate. Increasing image integration times is frequently not an option as the required dose may alter (damage) many samples of interest. Increases in either the frame rate or in the resolution in terms of number of pixels per frame will require improvements in DQE and possibly also new designs for the illumination systems of microscopes to maximize beam current. Mooney et al. (2011) have recently reported that silicon active pixel sensor (APS) instead of scintillator/fiber optic assembly can improve the recording rate of 40 frames s^{-1} .

Recently, a group of researchers at Lawrence Livermore National Laboratory have modified the TEM column to incorporate laser pulses to initiate a transient process to be investigated, e.g., phase transformations or chemical reactions, and timed it with the electron probe, also stimulated by a laser pulse, precisely such that snap shots can be recorded with 15 ns temporal resolution (King [et al.](#) and [Stuart](#), 2005). This microscope has been successfully employed to understand thermal annealing processes in thin films and the laser ablation mechanism for synthesis of nanowires (Kim [et al.](#) 2008).

The temporal resolution that can be achieved for spectroscopy is generally lower than that for imaging: 2 s to 10 s or more compared to 0.34 s for video imaging. Therefore, spectroscopy techniques are often used to analyze a sample before and after a reaction, unless the process is sufficiently slow. However, the recent introduction of a new generation of the imaging energy filters has enabled the efficient collection of spectra at rates of up to 100 s^{-1} is beginning to help overcome this limitation.

6. Limitations of *in situ* observations:

Limitations of *in situ* TEM characterization include the effect of the electron beam and poor sampling data that lead to poor statistics. Moreover, as samples suitable for TEM are usually of nanometer-scale thickness they may not represent the reaction mechanisms as they occur in bulk materials. Also, the reactions conditions, such as temperature and pressure that can be produced in the TEM may not represent the real-life situation. Therefore, it is important to verify the thermodynamic and kinetic parameters using other techniques such as X-ray diffraction,

thermogravimetric analysis, Raman spectroscopy, etc. Also, the structure and chemistry of reactants and products subjected to the same reaction conditions as used in the TEM should be tested on bulk samples.

It is also important to keep in mind that we cannot follow each and every chemical reaction using *in situ* TEM related techniques. Some examples of potential pitfalls are:

1. Electron beam effects: We should always be aware of the fact that electron beam can induce or change the reaction mechanism. Therefore observations should be made with and without electron beam radiations. We should also compare *in situ* observations with *ex situ* experiments.
2. Corrosive gases: Reactions involving corrosive gases, such as NO_x, SO_x, H₂S, halogens (F, Cl, Br, as reactant or products) will corrode the materials currently being used in TEM columns and holders.
3. Thermodynamic conditions: Currently the heating holders as well as the microscope configuration limit the achievable sample temperatures and pressure. For example, although samples can be heated up to 1500 °C using filament heating holders, current differentially pumped TEM designs limit the highest temperature to be 900 °C as the heat transfer through gases (via convection) is higher than in vacuum (via radiation).
4. Reaction kinetics: Observable reaction rates are dependent upon our recording media. Therefore, any reaction occurring faster than the recording rate cannot be captured. Currently this limit for imaging is $\approx 1/30$ s and EDS is ≈ 20 s. However, there are some recent developments that may help in resolving this limitation. For example, Kim et al have recently reported a different modification to capture faster reaction rates by

combining pulse heating with a pulsed electron beam (Kim, ~~Kwon~~ et al. 2008). GIF cameras capable of recording 100 energy-loss spectra/s have recently been introduced but real time data is still not available to confirm the practical feasibility for obtaining data with good signal to noise ratio for nanoparticles. On the other hand, *in situ* measurements are not suitable to follow reaction processes that take weeks or months such as the effect of thermal cycles on materials used in solid oxide fuel cells or the deactivation of catalysts after multiple cycles.

5. Heating holders: Heating holders are an essential component for the *in situ* observation of chemical reactions, as most of them require elevated temperatures. The current status of heating holders poses a limit to the achievable reaction temperature. Other issues with currently available commercial heating holders are lack of control on heating and cooling rate, and thermal drift, that make it difficult to collect good quality data. For example, samples continue to drift due to expansion of various components for 15 min to 20 min after reaching the temperature. Therefore high-resolution images or nanoscale spectroscopy cannot be recorded during this period making it quite difficult to obtain temperature-resolved data. Some new commercial designs to overcome some of these difficulties have been reported recently (Allard [et al.](#), 2009).

6. Acknowledgements

Stimulating discussions and collaborations with Prof. Crozier, Dr. Chee, Prof. Drucker, Dr. Diaz, Dr. Hoffman, Prof. Rez are gratefully acknowledged. Assistance from Mr. Karl Weiss has been

invaluable in the setting up *in situ* experiments at of John Cowley Center for High Resolution Electron Microscopy of Arizona State University.

Disclaimer:

The full description of the procedures used in the lecture notes requires the identification of certain commercial products and their suppliers. The inclusion of such information should in no way be construed as indicating that such products or suppliers are endorsed by NIST or are recommended by NIST or that they are necessarily the best materials, instruments, software or suppliers for the purposes described.

(1998). Microscopy and Microanalysis **4**.

(1998). Microscopy Research & Technique. **42**(4).

(2005). Journal of Materials Research **20**(7).

(2008). Mrs Bulletin **33**(2).

(2009). Microscopy Research & Technique **72**.

~~Ahn CC, K. O. (1983). "EELS Atlas." Arizona State University, HREM Facility and Gatan Inc., Tempe, Arizona.~~

Aikawa, S., ~~Kizu, T., Nishikawa, E. T. Kizu, et al.~~ (2010). "Catalytic graphitization of an amorphous carbon film under focused electron beam irradiation due to the presence of sputtered nickel metal particles." Carbon **48**(10): 2997-2999.

Alani, R. and M. Pan (2001). In situ transmission electron microscopy studies and real-time digital imaging, Blackwell Science Ltd.

Allard, L. F., Bigelow, W. C., Jose-Yacamán, M., Nackashi, D. P., Damiano, J., Mick, S. E. (2009). "A New MEMS-Based System for Ultra-High-Resolution Imaging at Elevated Temperatures." Microscopy Research and Technique **72**(3): 208-215.

Anton, R. (2008). "On the reaction kinetics of Ni with amorphous carbon." Carbon **46**(4): 656-662.

Barnhart, F., Ed. (2008). In-Situ Electron Microscopy at High Resolution. New Jersey, London, Singapore, Beijing, Hong Kong, Taipei, Chennai, World Scientific.

Bevan, D. J. M. (1955). "Ordered intermediate phases in the system CeO₂-Ce₂O₃." Journal of Inorganic and Nuclear Chemistry **1**: 49-59.

Bovin, J. O. and J. O. Malm (1991). "ATOMIC RESOLUTION ELECTRON-MICROSCOPY OF SMALL METAL-CLUSTERS." Zeitschrift Fur Physik D-Atoms Molecules and Clusters **19**(1-4): 293-298.

Chen, C. L. and H. Mori (2009). "In situ TEM observation of the growth and decomposition of monoclinic W18O49 nanowires." Nanotechnology **20**(28): 6.

Creemer, J. F., Helveg, S., Hoveling, G. H., Ullmann, S., Molenbroek, A. M., Sarro, P. M., Zandbergen, H. W., (2008). "Atomic-scale electron microscopy at ambient pressure." Ultramicroscopy **108**(9): 993-998.

- Crozier, P. A. and S. Chenna (2011). "In situ analysis of gas composition by electron energy-loss spectroscopy for environmental transmission electron microscopy." Ultramicroscopy **111**(3): 177-185.
- Diaz, R. E., Sharma, R., Jarvis, K., Mahajan, S. (2012). "Direct observation of nucleation and early stages of growth of GaN nanowires." J. Crystal Growth **341**: 1-6.
- Gai, P. L. (1999). "Environmental high resolution electron microscopy of gas-catalyst reactions." Topics in Catalysis **8**: 97-113.
- Gai, P. L., and Boyes, E.D. (2003). Electron Microscopy of heterogeneous catalysis. Series in Microscopy and Materials Science. Bristol, Philadelphia, Institute of Physics Publishing.
- Gajdardziska-Josifovska, M., Plass, Richard, Schofield, Marvin A., Geise, Daniel R., and Sharma, Renu (2002). "*In Situ* and *ex situ* electron microscopy studies of polar oxide surfaces with rock-salt structure." Journal of Electron Microscopy **51**(S): 513-525.
- Gamalski, A. D., Tersoff, J., Sharma, R., Ducati, C., Hofmann, S., (2010). "Formation of Metastable Liquid Catalyst during Subeutectic Growth of Germanium Nanowires." Nano Letters **10**(8): 2972-2976.
- Hofmann, S., Sharma, R., Wirth, C.T., Cervantes-Sodi, F., Ducati, C., Kasama, T., R. E. Dunin-Borkowski, Drucker, J., Bennet, P., Robertson, J. (2008). "Ledge-flow controlled catalyst interface dynamics during Si nanowire growth." Nature Materials **7**(5): 372-375.
- <http://www.marcorubber.com/viton.htm>.
- Kamino, T., Saka, H. (1993). "Newly developed high resolution hot stage and its applications to materials science " Microscopy, Microanalysis and Microstructure **4**: 127-135.
- Kamino, T., Yaguchi, T., Konno, M., Watabe, A., Marukawa, T., Mima, T., Kuroda, K., Saka, H., Arai, S., Makino, H., Suzuki Y., and Kishita K. (2005). "Development of a gas injection/ specimen heating holder for use with transmission electron microscope." Journal of Electron Microscopy **54**(6): 497-503.
- Kim, J. S., LaGrange, T., Reed, B. W., Taheri, M. L., Armstrong, M. R., King, W. E., Browning, N. D., Campbell, G. H. (2008). "Imaging of transient structures using nanosecond in situ TEM." Science **321**(5895): 1472-1475.
- Kim, T., [Kwon, S.](#), [Yoon, H.](#), [Chung, C.](#), [Kim, J.](#), [S. Kwon, et al.](#) (2008). "Fabrication of carbon nanotube paste using photosensitive polymer for field emission display." Colloids and Surfaces a-Physicochemical and Engineering Aspects **313**: 448-451.
- King, W. E., Campbell, G.H., Frank, A., Reed, B., Schmerge, J.F., Siwick, B.J., and B. C. Stuart, Weber, P.M. (2005). "Ultrafast electron microscopy in materials science, biology, and chemistry." Journal of Applied Physics **97**: 111101.
- Kodambaka, S., Tersoff, J., Reuter, M. C., Ross, F. M., (2006). "Diameter-independent kinetics in the vapor-liquid-solid growth of Si nanowires." Physical Review Letters **96**(9).
- Kodambaka, S., Tersoff, J., Reuter, M. C., Ross, F. M. (2007). "Germanium nanowire growth below the eutectic temperature." Science **316**(5825): 729-732.
- Kojima, Y., Kasuya, K., Nafato, K., Hamaguchi, T., Nakao, M., (2008). "Solid-phase growth mechanism of tungsten oxide nanowires synthesized on sputtered tungsten film. Journal of Vacuum Science and Technology B **26**, 1942-1947." Journal of Vacuum Science & Technology **B26**: 1942-1947.

- Lascelles, K. and L. V. Renny (1983). "THE RATE OF FORMATION OF NICKEL CARBONYL FROM CARBON-MONOXIDE AND NICKEL SINGLE-CRYSTALS." Surface Science **125**(2): L67-L72.
- Litwiller, D. (2005). "CMOs vs. CCD: Maturing technologies, maturing markets." Photonics Spectra **39**(8): 54-+.
- Mooney, P. E., Contarato, D., Denes, P., Gubbens, A.J., Lee, Lent, B., M., Agard, D.A. (2011). "A High-Speed Electron-Counting Direct Detection Camera for TEM." Microsc. Microanal. **17** ((Suppl 2)): 1004-1005.
- Okamoto, H. (1995). "Pt-Si." Journal of Phase Equilibria **16**(3): 286-287.
- Richardson, J. T., Lei, M., Forster, K., Twigg, M. V., (1994). "REDUCTION OF MODEL STEAM REFORMING CATALYSTS - NiO/ALPHA-AL₂O₃." Applied Catalysis a-General **110**(2): 217-237.
- Robertson, I. M., Teter, D. (1998). "Controlled Environment Transmission Electron Microscopy." Microscopy Research & Technique **42**(4): 260-269.
- Ross, F. M., Tromp, R. M., Reuter, M. C., (1999). "Transition states between pyramids and domes during Ge/Si island growth." Science **286**(5446): 1931-1934.
- Sahle, W. and S. Berglund (1981). "THE MORPHOLOGY OF SLIGHTLY REDUCED TUNGSTEN TRIOXIDE EQUILIBRATED WITH CO-CO₂ GASEOUS BUFFERS WITH AND WITHOUT WATER ADDITION." Journal of the Less-Common Metals **79**(2): 271-280.
- Schoen, D. T., Peng, H. L., Cui, Y., H. L. Peng, et al. (2009). "Anisotropy of Chemical Transformation from In₂Se₃ to CuInSe₂ Nanowires through Solid State Reaction." Journal of the American Chemical Society **131**(23): 7973-7975.
- Sharma, R. (2005). "An environmental transmission electron microscope for in situ synthesis and characterization of nanomaterials." Journal of Materials Research **20**(7): 1695-1707.
- Sharma, R., and Weiss, K. (1998). "Development of a TEM to study in situ structural and chemical changes at atomic level during gas solid interaction at elevated temperatures." Microscopy Research & Technique **42**(4): 270-280.
- Sharma, R., Chee, S. W., Herzing, A., Miranda, R., Rez, P., (2011). "Evaluation of the Role of Au in Improving Catalytic Activity of Ni Nanoparticles for the Formation of One-Dimensional Carbon Nanostructures." Nano Letters **11**(6): 2464-2471.
- Sharma, R., Crozier, Peter A. (2005). Environmental Transmission Electron Microscopy in Nanotechnology. Transmission Electron microscopy for nanotechnology. N. Y. Z. L. Wang, Springer-Verlag and Tsinghua University Press: 531-565.
- Sharma, R., Crozier, Peter A., Kang Z.C., and Eyring, L. (2004). "Observation of dynamic nanostructural and nanochemical changes in Ceria-based catalysts during in situ reduction." Philosophical Magazine **84**: 2731-2747.
- Sharma, R., Moore, E.S., Rez, P., Treacy M.M.J. (2009). "Site-specific fabrication of Fe particles for carbon nanotube growth." Nano Letters **9**(2): 689-694.
- Stach, E. A. (2008). "Real-time observations with electron microscopy." Materials Today **11**: 50-58.
- Takahashi, Y., H. Ishii, J. Murota, . (1985). "NEW PLATINUM SILICIDE FORMATION METHOD USING REACTION BETWEEN PLATINUM AND SILANE." Journal of Applied Physics **58**(8): 3190-3194.
- White, A. H., Melville, W. (1905). "THE DECOMPOSITION OF AMMONIA AT HIGH TEMPERATURES." Journal of American Chemical Society **27**(4): 373-386.

Yao, N., Wang, Zhong L., Ed. (2005). Handbook of Microscopy for Nanotechnology. Boston, Dordrecht, New York, London, Kluwer Academic Publishers.
Zhang, Z. L. and D. S. Su (2009). "Behaviour of TEM metal grids during in-situ heating experiments." Ultramicroscopy **109**(6): 766-774.

Table1. Thermal conductivity of selected gasses and gas mixtures.

Gas	μ_g ($Wm^{-1}K^{-1}$)
H ₂	1684
H ₂ O	158
He	1415
N ₂	243
O ₂	151
CO	232
Ar	162
5mol/mol H ₂ in Ar	237
5mol/mol H ₂ in N ₂	314

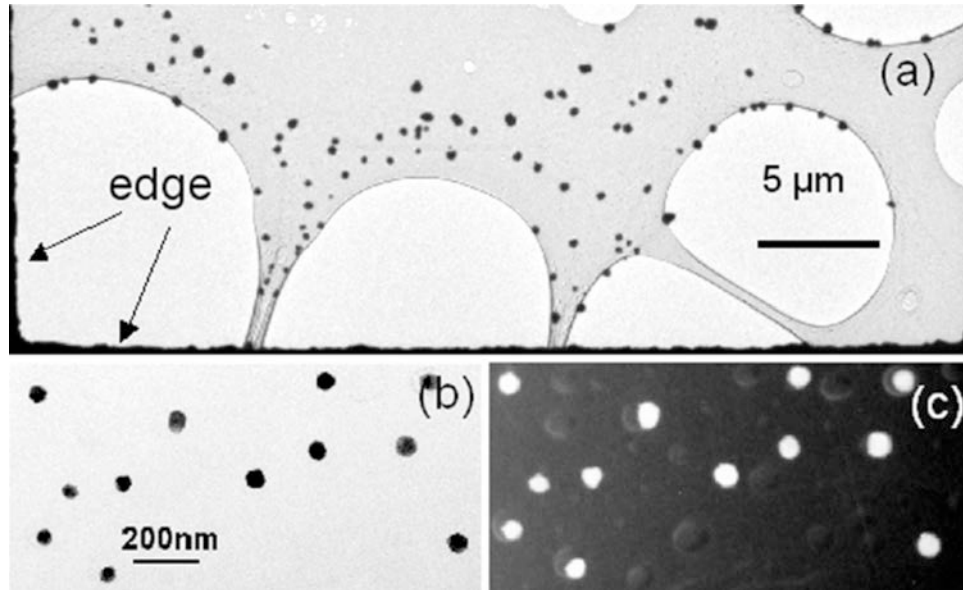


Figure 1. (a) TEM image of amorphous carbon film supported on Cu grid after *in situ* heating at 600 C for 0.2 h. (b-c) Higher magnification bright-field and dark-field images showing the formation of metallic Cu particles. (Zhang and Su)

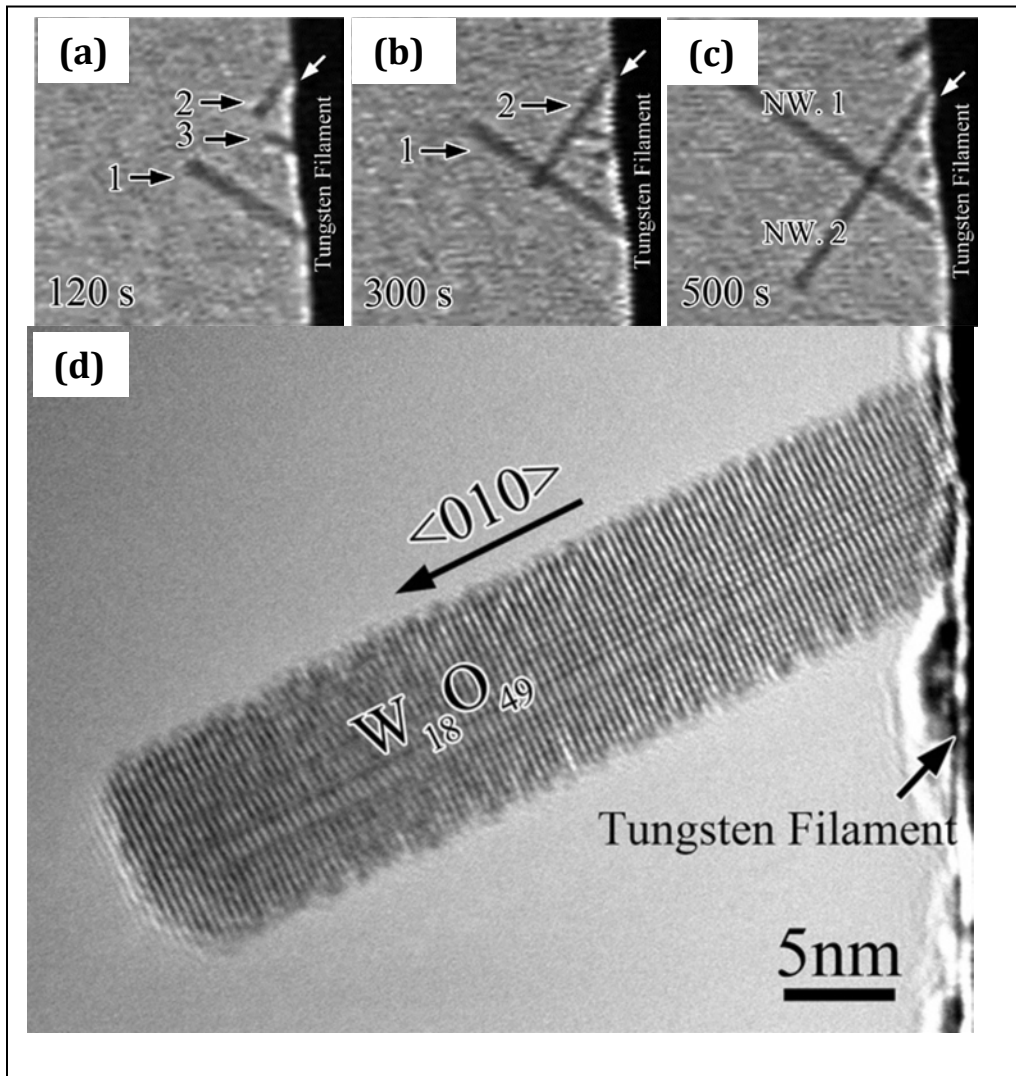


Figure3. Time resolved TEM images recorded after (a) 120 s, (b) 300 s, and (500 s) showing the growth nanowires from the tungsten filament heating holder at 600 °C. (d) High resolution image from the nanowire confirm them to have $W_{18}O_{49}$ structure and growth direction to be $\langle 010 \rangle$. (Chen and Mori 2009)

2011) (Crozier and Chenna 2011) (Crozier and Chenna 2011) (Crozier and Chenna 2011)
(Crozier and Chenna 2011) (Crozier and Chenna 2011) (Crozier and Chenna 2011) (Crozier
and Chenna 2011) (Crozier and Chenna 2011) (Crozier and Chenna 2011)

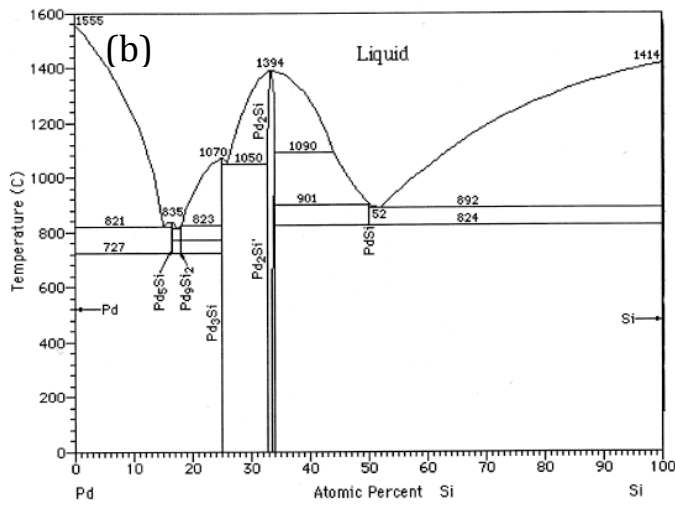
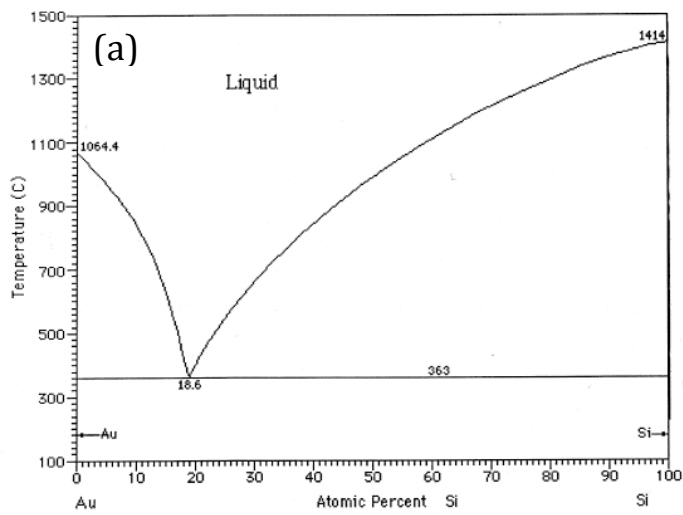


Figure 5. Si-Au and Si-Pd phase diagrams

(source: http://www.crct.polymtl.ca/FACT/documentation/SGTE/SGTE_Figs.htm)

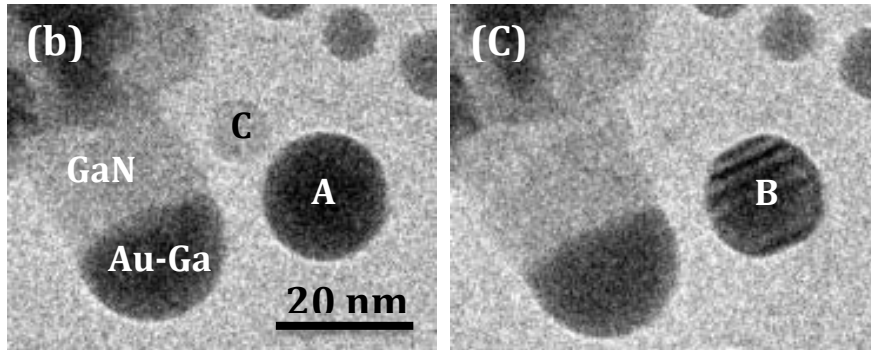
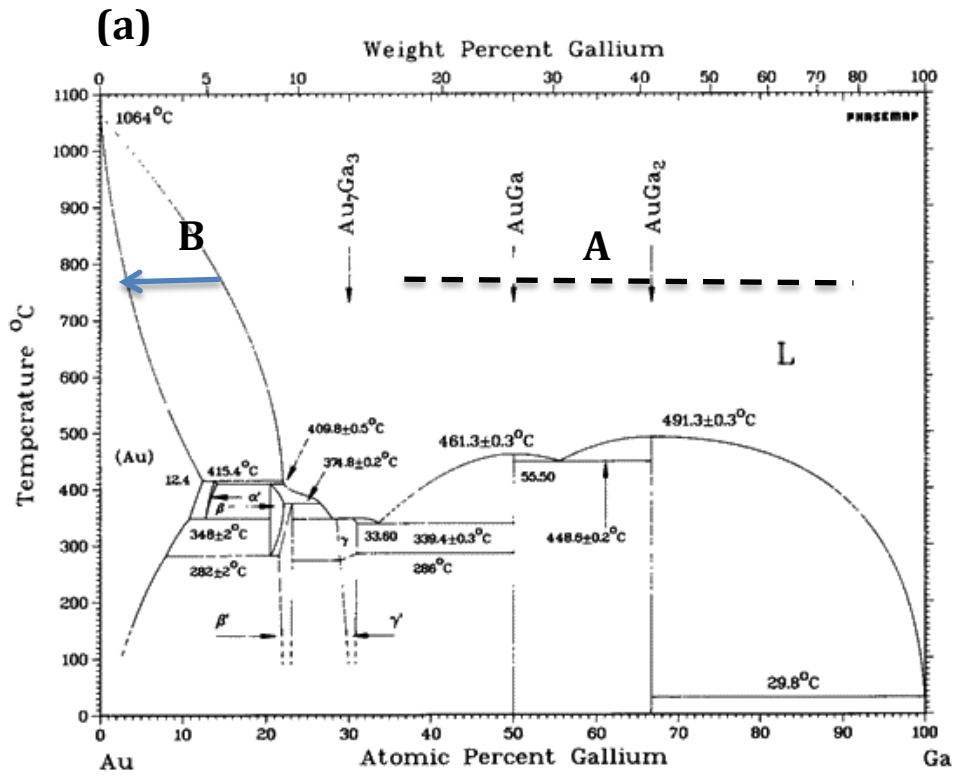


Figure 6. (a) Au-Ga Phase diagram showing the liquidus region (A) and start of solidification in the Au rich region (B). (b-c) Experimental images extracted from a video recorded during GaN nanowire nucleation and growth at 800 °C in 0.2 Pa of flowing NH₃. (b) Liquid particle marked A, with Ga-Au composition corresponding to the region A in the phase diagram, (c) became solid after coalescing with another particle (marked C). The solidification of the particle indicates that coalescence of the two particles changed the composition of the particle in the region marked (B) in the phase diagram.